Biosensors and Bioelectronics 111 (2018) 144–151

Contents lists available at ScienceDirect

Biosensors and Bioelectronics

journal homepage: www.elsevier.com/locate/bios

Electrochemical biointerfaces based on carbon nanotubes-mesoporous silica hybrid material: Bioelectrocatalysis of hemoglobin and biosensing applications

Marcos Eguílaz[a,*], Reynaldo Villalonga[b], Gustavo Rivas[a,*]

[a] INFIQC, Departamento de Físicoquimica, Facultad de Ciencias Químicas, Universidad Nacional de Córdoba, 5000 Córdoba, Argentina
[b] Nanosensors & Nanomachines Group, Department of Analytical Chemistry, Faculty of Chemistry, Complutense University of Madrid, 28040 Madrid, Spain

ARTICLE INFO

Keywords:
Hybrid materials
Carbon nanotubes
Mesoporous silica
Hemoglobin
Trichloroacetic acid
Nitrite

ABSTRACT

We are reporting a novel biosensing platform based on a hybrid nanomaterial that combines the advantages of Nafion-coated multiwalled carbon nanotubes (MWCNTs) and mesoporous silica MCM41 nanoparticles functionalized with hemoglobin (Hb). MWCNTs-MCM41-Hb hybrid bioconjugate was characterized by scanning electron microscopy (SEM), UV–vis spectroscopy and electrochemical techniques after deposition at glassy carbon electrodes (GCE). The combination of the high surface area, biocompatibility and protein loading capacity of MCM41 nanoparticles and the high surface area and catalytic properties of MWCNTs allowed the direct electron transfer (DET) between Hb and the electrode surface. The electron transfer rate constant (k) and the surface coverage of electroactive Hb (Γ_{Hb}) were 5.2 s^{-1} and 4.7 × 10^{-10} mol cm^{-2}, respectively. The GCE modified with the nanostructured architecture (GCE/MWCNTs-MCM41-Hb) was successfully used as a third-generation biosensor for the highly sensitive and selective quantification of nitrite (NO_2^-) and trichloroacetic acid (TCA) by taking advantage of the excellent biocatalytic activity of Hb and the efficient direct charge transfer of the heme group.

1. Introduction

The search for novel electrochemical interfaces able to conjugate an efficient immobilization of biomolecules with an improved electroanalytical performance in terms of sensitivity, selectivity, transducer response, and real applicability, is an important challenge in the field of advanced electrochemical biosensors (Everson et al., 2017). In this context, due to their unique physicochemical properties, the nano/micro-structured materials have received great attention for the development of innovative electrochemical biosensing surfaces with optimal architecture and suitable structural and electronconductive characteristics (Ding et al., 2013; Everson et al., 2017; Qu et al., 2016; Walcarius et al., 2013; Wang et al., 2017a; Zhu et al., 2015). In particular, carbon nanotubes (CNTs) have demonstrated to play a relevant role for such a purpose due to their high chemical stability and excellent electronic and mechanical properties that made possible the building of modified electrodes with improved electroanalytical performance (Yang et al., 2015a, 2015b).

Mesoporous silica-based materials have also attracted considerably attention for the development of electrochemical (bio)sensors due to their functionalizable and large specific surface area, mechanical stability, biocompatibility, and three-dimensional structure made of highly open interconnected spaces (Hasanzadeh et al., 2013, 2012). Nevertheless, even when the silica-based materials present several of the properties desired for the construction of chemically modified electrodes, most of these materials are electronic insulators with low charge transfer efficiency. Therefore, the incorporation of an additional material is commonly required to be used for electrochemical applications (Walcarius et al., 2005). For example, silica-based materials have been successfully combined with graphite (Khan et al., 2016), gold nanoparticles (Iminova et al., 2015), ZnO quantum dots (Pabbi and Mittal, 2017) and reduced graphene oxide (Abraham et al., 2015) to develop electrochemical biosensors. In this context, biosensing devices prepared with hybrid materials constituted by two or more components have demonstrated better biocompatibility, stability and sensitivity than similar configurations using the individual components due to the combined properties or synergistic effect of the individual materials (Eguílaz et al., 2015, 2011). Silica nanoparticles have been also used to amplify the analytical signal obtained during different biosensing schemes. For instance, Zhao et al. reported the ultrasensitive electrochemical immunosensing of human immunoglobulin G based on the use of horseradish peroxidase-loaded silica-poly(acrylic acid) brushes as

* Corresponding authors.
E-mail addresses: mrubio@fcq.unc.edu.ar (M. Eguílaz), grivas@fcq.unc.edu.ar (G. Rivas).

https://doi.org/10.1016/j.bios.2018.04.004
Received 17 January 2018; Received in revised form 29 March 2018; Accepted 3 April 2018
Available online 04 April 2018
0956-5663/

labels (Zhao et al., 2016).

The direct electron transfer (DET) between proteins redox centers and electrode surfaces and its application for the development of third-generation electrochemical biosensors has received great attention (Das et al., 2016; Taurino et al., 2016). The critical points in the design of electrochemical biosensors based on DET are connected with the distance between the prosthetic group of the inmobilized redox protein and the electrode surface, and the stable and oriented immobilization of the protein preserving its 3D-structure (Das et al., 2016). In this sense, nanomaterials have demonstrated to be very useful for this task due to their unique structural and electronic properties (Bagheri et al., 2016; Eguílaz et al., 2016; Wang et al., 2017b).

In this work, we present a novel hybrid nanomaterial that combines the advantages of Nafion-coated multiwalled carbon nanotubes (MWCNTs) and mesoporous silica MCM41 nanoparticles functionalized with hemoglobin (Hb) (MWCNTs-MCM41-Hb) to develop biosensing platforms based on the direct electron transfer of the hemoglobin immobilized at silica nanoparticles. To the best of our knowledge, this is the first report on the use of this hybrid material to develop third-generation biosensors. So far, only a nanohybrid biosensor based on MWCNTs, AuNPs and silica nanoparticles, developed for the detection of methyl parathion (Ye et al., 2016), and a nanocomposite material of single-walled carbon nanotubes (SWCNTs) and gold-mesoporous silica Janus nanoparticles developed for the bienzymatic glucose biosensing (through the use of glucose oxidase (GOx), horseradish peroxidase (HRP) and hydroquinone as redox mediator) have been developed (Boujakhrout et al., 2015). The use of MWCNTs coated with mesoporous silica as signal tag for the electrochemical aptasensing of thrombin (Zhang et al., 2013) and mucin 1 (Chen et al., 2014) has been aso reported.

In the following sections we report the preparation, optimization and characterization of a MWCNTs-MCM41-Hb hybrid bioconjugate by scanning electron microscopy (SEM), UV–vis spectroscopy and electrochemical techniques once deposited at glassy carbon electrodes (GCE); and the analytical application of GCE/MWCNTs-MCM41-Hb as third-generation biosensor for the quantification of two known substrates of Hb like nitrite and trichloroacetic acid (TCA) ~~quantification~~.

2. Experimental

2.1. Chemicals and solutions

Multi-walled carbon nanotubes (MWCNTs, (30 ± 15) nm diameter, (1 − 5) μm length and purity higher than 95%), were supplied from Nanolab (USA). Mesoporous silica particles MCM41 (MCM41, (102 ± 5) nm particle size, 2.1 nm pore size) were provided by Orion High Technologies (Spain). Human hemoglobin (Hb), hydroquinone and Nafion perfluorinated solution were supplied by Sigma. Hydrogen peroxide (30% v/v aqueous solution), NaH_2PO_4 and Na_2HPO_4 were purchased from Baker. Sodium nitrite and trichloroacetic acid (TCA) were obtained from Biopack. Other chemicals were of analytical grade and used without further purification.

A 0.050 M phosphate buffer solution pH 7.00 was employed as supporting electrolyte. Ultrapure water (ρ = 18.2 MΩ cm) from a Millipore-MilliQ system was used for preparing all aqueous solutions.

2.2. Apparatus

Sonication treatments were carried out with an ultrasonic processor VCX 130 W (Sonics and Materials, Inc.), of 20 kHz frequency with a titanium alloy microtip (3 mm diameter). A Digicen 21 ultracentrifuge (Orto Alresa) with a RT 151 rotor was used to centrifuge the samples after sonication.

UV–vis absorption spectra were obtained with a Shimadzu UV-1700 Pharma spectrophotometer using a quartz cuvette of 1 mm path length. Scanning Electron Microscopy (SEM) images were obtained with a Field Emission Gun Scanning Electron Microscope (FE-SEM, Zeiss,ΣIGMA model) equipped with secondary and back-scattered electron detectors. For this purpose, samples were prepared by drop-coating of hybrid dispersions onto GCE disks and solvent evaporation at room temperature.

Electrochemical experiments were carried out with a TEQ_04 potentiostat. Glassy carbon electrodes (GCE, CH Instruments, 3 mm diameter), and hybrid modified-GCE were used as working electrodes. A platinum wire and Ag/AgCl, 3 M NaCl (BAS, Model RE-5B) were used as auxiliary and reference electrodes, respectively. All potentials are referred to this reference electrode. A magnetic stirrer under controlled speed provided the convective transport during the amperometric measurements.

2.3. Preparation of MWCNTs-MCM41-Hb hybrid bioconjugate

2.3.1. MCM41-Hb

MCM41-Hb bioconjugate was prepared by mixing 2.0 mg of MCM41 and 1.0 mL of a 0.50 mg mL^{-1} Hb solution (in a 0.050 M phosphate buffer solution pH 7.00) with magnetic stirring in ice-bath for 1.0 h. The resulting bioconjugate was isolated by centrifugation, washed twice with 0.050 M phosphate buffer solution pH 7.00 and resuspended in the appropriate volume of the phosphate buffer solution to obtain a 20.0 mg mL^{-1} MCM41-Hb suspension (Fig. 1A).

2.3.2. MWCNTs-Nafion

The dispersion of MWCNTs was prepared by mixing 1.0 mg of MWCNTs with 1.0 mL of 0.1% (v/v) Nafion (diluted in water) followed by sonication with a sonicator probe for 15 min (amplitude of 60%) while keeping the mixture in an ice-bath. After this treatment, the resulting dispersion was centrifuged at 4000 rpm for 15 min to remove the aggregates of MWCNTs (Fig. 1B).

2.3.3. MWCNTs-MCM41-Hb

MWCNTs-MCM41-Hb hybrid bioconjugate was prepared by mixing MWCNTs-Nafion dispersion and MCM41-Hb suspension in a 90/10 (v/v) ratio with the help of a vortex (Fig. 1C). For comparison, MWCNTs, MCM41 and MCM41-Hb materials were prepared using similar conditions.

2.4. Preparation of glassy carbon electrodes modified with MWCNTs-MCM41-Hb hybrid bioconjugate

GCEs were polished with alumina slurries of 1.0, 0.3 and 0.05 μm for 1 min each, rinsed thoroughly with deionized water, sonicated for 30 s in water, and finally dried under a N_2 stream. After that, 10 μL of MWCNTs-MCM41-Hb bioconjugate was deposited at the GCE followed by evaporation of the solvent at room temperature. GCE/MWCNTs-MCM41-Hb biosensor was rinsed with ultrapure water before using (Fig. 1D). For comparison, GCE/MCM41, GCE/MCM41-Hb, GCE/MWCNTs and GCE/MWCNTs-Hb were also prepared following the same scheme. The electroactive area of the electrodes was obtained by cyclic voltammetry using 5.0×10^{-4} M hydroquinone.

2.5. Procedure

The electrochemical experiments were performed in a N_2-saturated 0.050 M phosphate buffer solution pH 7.00. Cyclic voltammetry (CV) experiments were carried out between 0.300 V and − 1.000 V at a scan rate of 0.100 Vs^{-1}. Amperometric experiments for NO_2^- and TCA determination were performed in stirred solutions by applying − 0.100 V as working potential and allowing the transient current to reach a steady-state value prior to the addition of the analyte and subsequent current monitoring. All experiments were conducted at room temperature.

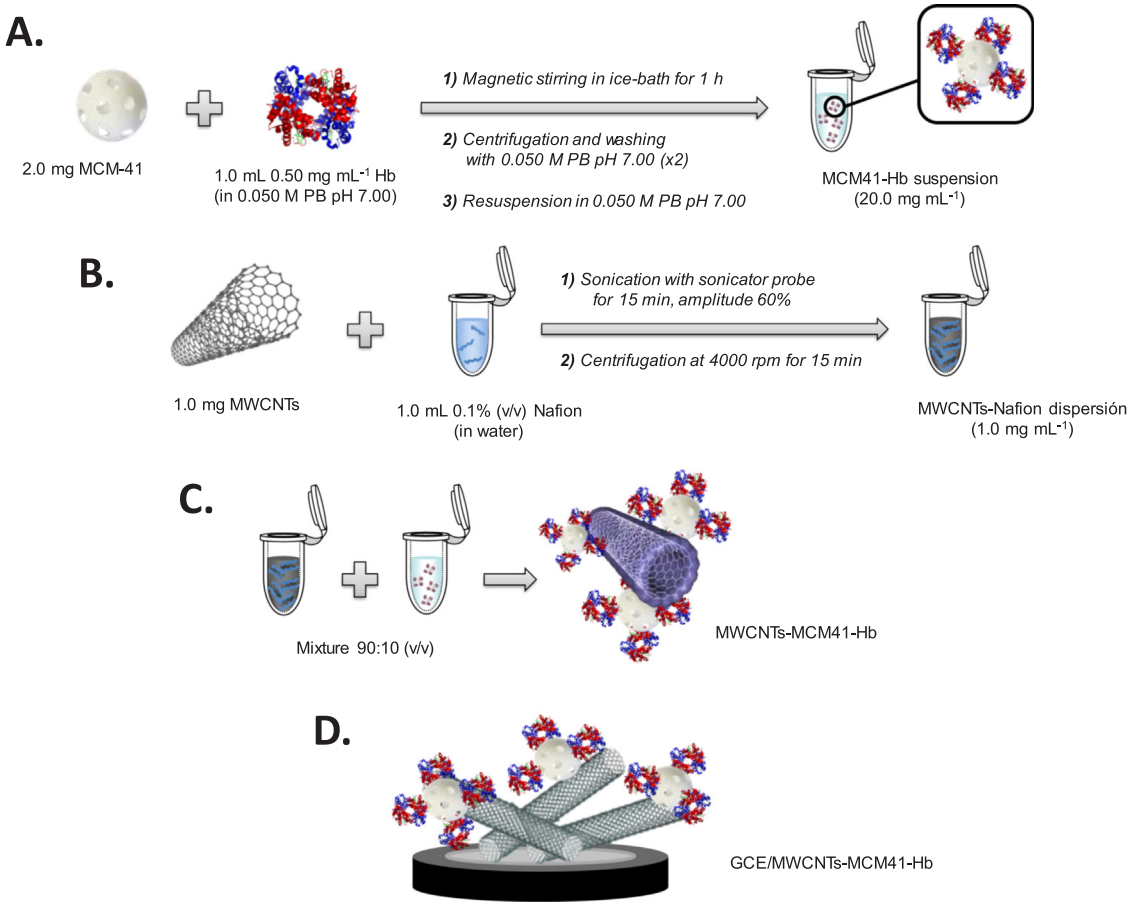

Fig. 1. Schematic representation of the steps involved in the preparation of the GCE/MWCNTs-MCM41-Hb bioplatform.

2.6. Determination of NO_2^- and TCA in real samples

The tap water was obtained from a restaurant at Cordoba National University Campus and used without any pretreatment. Since NO_2^- and TCA were not detected in the sample, we evaluated the recovery of these analytes by spiking the tap water samples. The determinations were performed by amperometry at − 0.100 V in the N_2-saturated 0.050 M phosphate buffer solution pH 7.00.

3. Results and discussion

3.1. Characterization of MCM41-Hb hybrid bioconjugate

UV–vis spectroscopy is a useful tool to study the interaction between Hb and MCM41 particles since the position and intensity of the characteristic Soret band of hemeproteins are sensitive to the microenvironment of the heme site (Chen et al., 2016; Eguílaz et al., 2016). Fig. 2A shows the UV–vis spectra for native Hb (a), MCM41 suspension (b) and MCM41-Hb bioconjugate (c) prepared in a 0.050 M phosphate buffer solution pH 7.00. The spectrum of native Hb shows the typical Soret band at 406 nm (Baccarin et al., 2015; Feng et al., 2011). No absorption bands are observed in the spectrum of MCM41 suspension. MCM41-Hb bioconjugate spectrum displays the Soret band, confirming the immobilization of the hemeprotein at MCM41 particles. The slight red-shift in the wavelength of maximum absorption (409 nm) compared to the native Hb (406 nm) could be associated with some degree of denaturation of the protein and its interaction with MCM41 due to the high surface potential energy and adsorption properties of this nanomaterial (Dai et al., 2004; Urabe et al., 2007).

The pH is a variable that affects the surface charge of mesoporous silica and the degree of Hb ionization in solution (Devineau et al., 2017; Moerz and Huber, 2015). Fig. 2B shows the maximum absorbance of the Soret band for MCM41-Hb bioconjugates prepared with Hb solutions of different pHs. This profile of absorbance versus pH shows that the maximum absorbance and, therefore, the maximum amount of Hb adsorbed at MCM41, are reached around pHs 6.00 and 7.00, indicating that these pHs represent the best compromise between the negative charge of MCM41 silica particles (Suteewong et al., 2011; Wu et al., 2013)) and the positive charge of Hb (Ghodsi et al., 2016). At pHs higher than the isoelectric point of Hb, the protein is negatively charged and its adsorption at negatively charged MCM41 particles becomes less favorable (Devineau et al., 2017). Therefore, pH 7.00 was selected for further work.

The interaction time between MCM41 and Hb has demonstrated to be an important parameter in the optimization of the biosensor. We evaluated the influence of this parameter from UV–visible experiments. Fig. 2C displays the variation of the amount of Hb immobilized at MCM41 as a function of the interaction time between 2.00 mg mL^{-1} MCM41 and 0.50 mg mL^{-1} Hb. This amount was obtained from the difference between the maximum absorbance of Soret band for the Hb solution before and after the interaction with MCM41 nanoparticles and separation of MCM41-Hb. The amount of Hb immobilized at MCM41 silica particles increases up to 1 h and then it remains almost constant indicating a saturation of the anionic siloxide groups of MCM41. Under the optimum conditions (2.0 mg mL^{-1} MCM41 particles mixed with 0.50 mg mL^{-1} Hb for 1 h), the amount of immobilized Hb was 0.20 mg per mg of MCM41. The effect of Hb concentration on the adsorption of MCM41 was also evaluated (not shown). Since no changes were observed between 0.50 and 4.00 mg mL^{-1} Hb, 0.50 mg mL^{-1} was selected for further work.

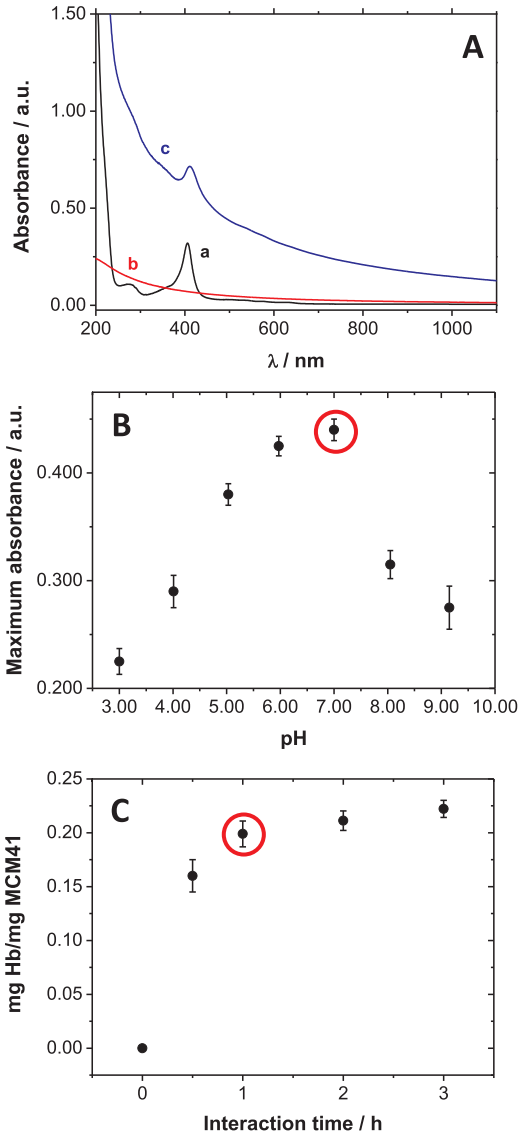

Fig. 2. (A) UV–vis absorption spectra for: (a) native Hb; (b) MCM41 suspension and (c) MCM41-Hb bioconjugate. (B) Variation of the maximum absorbance of the Soret band for MCM41-Hb bioconjugates as a function of the pH of Hb solutions value solutions. (C) Amount of immobilized Hb as a function of the incubation time in 0.50 mg mL^{-1} Hb solution.

3.2. Characterization of MWCNTs-MCM41-Hb hybrid bioconjugate

MWCNTs-MCM41-Hb bioconjugate was prepared by mixing Nafion-wrapped MWCNTs and MCM41-Hb in a ratio 90/10 v/v following the procedure described in the experimental section (See Fig. 1). SEM images of the resulting MWCNTs-MCM41-Hb hybrid bioconjugate deposited at glassy carbon disks show that the hybrid material covers the whole surface and MCM41-Hb particles are trapped in the three-dimensional network of carbon nanotubes (Fig. 3A). The inset displays a section with higher magnification where the intimate contact between MWCNTs and Hb-modified silica particles is clearly observed. Fig. 1-SI shows SEM images of glassy carbon disks modified with MWCNTs-Nafion (A) and MCM41 silica particles (B). As expected, the MWCNTs wrapped by the polymer completely covers the glassy carbon surface showing areas with higher density of MWCNTs. Fig S1-B clearly reveals the presence of silica nanoparticles, in general highly packed on the surface of the disk. The inset shows one area of the picture with higher magnification.

Fig. 3B shows cyclic voltammograms obtained in a N_2-saturated 0.050 M phosphate buffer solution pH 7.00 at 0.100 V s^{-1} at GCE/MCM41 (a), GCE/MWCNTs (b), GCE/MCM41-Hb (c), GCE/MWCNTs-MCM41-Hb (d) and GCE/MWCNTs-Hb (e). No peaks were observed neither at GCE/MCM41 (a) nor at GCE/MWCNTs (b). The i-E profiles for GCE/MCM41-Hb (c) shows a pair of assymetrical peaks with anodic-to-cathodic currents ratio (i_{ox}/i_{red}) of 0.58 (i_{ox} = 0.21 μA; i_{red} = − 0.36 μA), the cathodic one at – 0.365 V (E_{pc}) and the anodic one at – 0.346 V (E_{pa}), with a peak potential separation (ΔE_p) of 0.019 V, and a formal potential ($E^{0'}$) of – 355.5 mV. Since this peaks system is not observed at GCE/MCM41 (a), it is clearly due to the DET of the heme group of immobilized Hb, in agreement with the results previously reported for the DET of Hb immobilized on a hexagonal mesoporous silica (Dai et al., 2004), and for the DET of Hb at different mesoporous silica (Li et al., 2010). The potentiodynamic profile obtained at GCE modified with MWCNTs-MCM41-Hb hybrid bioconjugate (d) presents a pair of well-defined and symmetrical redox peaks with i_{ox}/i_{red} = 0.97 (i_{ox} = 2.92 μA; i_{red} = − 3.02 μA), E_{pc} = – 0.398 V, E_{pa} = – 0.367 V, ΔE_p = 0.031 V, $E^{0'}$ = – 382.5 mV. The enhancement in the peak currents observed at GCE/MWCNTs-MCM41-Hb compared to GCE/MCM41-Hb can be ascribed to the immobilization of a higher amount of MCM41-Hb at MWCNTs and to the better connection between the metalloprotein redox center and the nanomaterial. To verify the contribution of MCM41 particles, a control bioelectrode was prepared by immobilizing Hb directly at MWCNTs-modified GCE. The profiles at the resulting GCE/MWCNTs-Hb (e) show ΔE_p = 0.080 V, and peak currents 1.8-fold lower than those obtained at GCE/MWCNTs-MCM41-Hb. This behavior can be attributed to the immobilization of a lower amount of Hb immobilized on MWCNTs surface and the partial blocking of its conducting surface by the insulating hemeprotein.

To evaluate the effect of the amount of MCM41-Hb present in the mixture MWCNTs/MCM41-Hb, we prepared different MWCNTs-MCM41-Hb hybrid bioconjugates by varying the amount of MCM41-Hb. Fig. 3C shows cyclic voltammograms obtained in a N_2-saturated 0.050 M phosphate buffer solution pH 7.00 at 0.100 V s^{-1} at GCE modified with MWCNTs-MCM41-Hb dispersions prepared without MCM41-Hb (black) and with 0.50 mg mL^{-1} (red), 1.00 mg mL^{-1} (blue), 2.00 mg mL^{-1} (gray) and 5.00 mg mL^{-1} (orange) MCM41-Hb. The potentiodynamic profiles clearly show an increase in the peak currents as the amount of MCM41-Hb increases due to the presence of a higher amount of immobilized hemeprotein.

The effect of the scan rate on the peak currents for the different GCE/MWCNTs-MCM41-Hb bioelectrodes was also evaluated (Fig. 2A-SI). There is a linear relationship between the cathodic and anodic peak currents and the scan rate in the range between 0.010 and 0.500 V s^{-1} confirming that the electron transfer between the hemeprotein and the electrode is a surface-controlled quasi-reversible electrochemical process. The average surface concentration (Γ) of electroactive Hb present at the different GCE/MWCNTs-MCM41-Hb electrodes was estimated from the slope of i_p versus the scan rate, according to the following equation (Laviron, 1979a):

$$i_p = \frac{n^2F^2\nu\Gamma A}{4RT}$$

where ν is the scan rate, n is the number of the electrons involved in the redox process (n = 1 for Hb), F is the Faraday constant, A is the effective area of the electrode, R is the gas constant, and T is the temperature. Γ_{Hb} values of 6.0×10^{-11}, 1.8×10^{-10}, 4.7×10^{-10} and 9.5×10^{-10} mol cm^{-2} were obtained at GCE/MWCNTs-MCM41-Hb containing 0.50, 1.00, 2.00 and 5.00 mg mL^{-1} MCM41-Hb, respectively.

The electron transfer rate constants (k) were obtained by using Laviron´s model for a surface-controlled electrochemical system when the value of $n\Delta E_p \leq 200$ mV (n is the number of transferred electrons) (Laviron, 1979b):

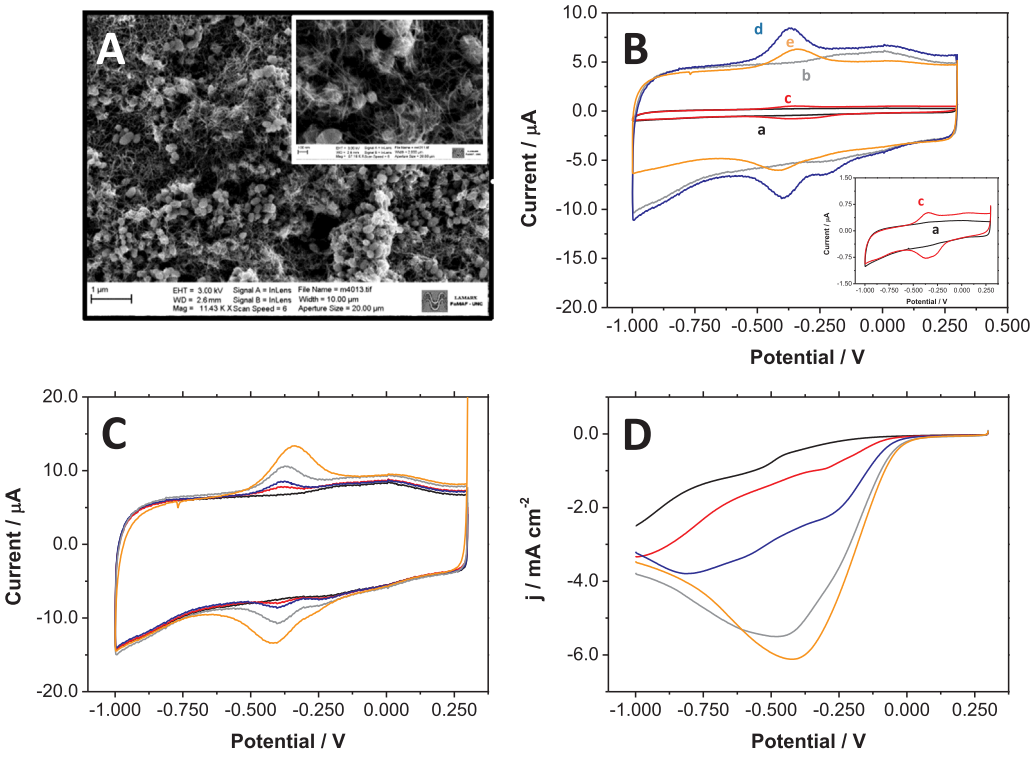

Fig. 3. (A) SEM micrograph of a glassy carbon disk modified with MWCNTs-MCM41-Hb hybrid bioconjugate. Magnification: 11430 ×. The inset shows a section of the surface with higher magnification (57160 ×). (B) Cyclic voltammograms obtained at GCE/MCM41 (a), GCE/MCM41-Hb (b), GCE/MWCNTs (c), GCE/MWCNTs-MCM41-Hb (d) and GCE/MWCNTs-Hb (e) in a N_2-saturated 0.05 M phosphate buffer solution pH 7.00 at 0.100 V s^{-1}. (C) Cyclic voltammograms obtained at GCE modified with MWCNTs (black) and at GCE modified with MWCNTs-MCM41-Hb using different amounts of MCM41-Hb: 0.50 mg mL^{-1} (red), 1.00 mg mL^{-1} (blue), 2.00 mg mL^{-1} (gray) and 5.00 mg mL^{-1} (orange). (D) Linear sweep voltammograms obtained using GCE/MWCNTs (black) and GCE/MWCNTs-MCM41-Hb electrode prepared with 0.50 mg mL^{-1} (red), 1.00 mg mL^{-1} (blue), 2.00 mg mL^{-1} (gray) and 5.00 mg mL^{-1} (orange) MCM41-Hb, in 1.0×10^{-2} M H_2O_2. Supporting electrolyte: N_2-saturated 0.050 M phosphate buffer solution pH 7 at 0.100 V s^{-1}. Scan rate: 0.100 V s^{-1}.(For interpretation of the references to color in this figure legend, the reader is referred to the web version of this article.)

$$m = \frac{RT}{nF}\frac{k}{v}$$

where m is a parameter related to ΔE_p. In correlation with the increase of ΔE_p with the scan rate obtained for electrodes containing different amounts of MCM41-Hb shown in the Fig. 2B-SI, the rate constants k (measured at 0.100 V) decrease for electrodes containing increasing amounts of MCM41-Hb. In fact, values of k of 7.7 s^{-1}, 7.7 s^{-1}, 5.2 s^{-1} and 1.4 s^{-1} were obtained for electrodes prepared with 0.50, 1.00, 2.00 and 5.00 mg mL^{-1} MCM41-Hb, respectively, indicating that the higher the amount of MCM41-Hb the slower the electron transfer due to the increment of the non-conductive silica nanoparticles and the relative smaller contribution of electro-conducting MWCNTs.

The biocatalytic activity of Hb confined at GCE/MWCNTs-MCM41-Hb containing different amounts of MCM41-Hb was evaluated using hydrogen peroxide as marker. Fig. 3D shows the linear sweep voltammograms obtained at GCE/MWCNTs (black) and at GCE/MWCNTs-MCM41-Hb prepared with MCM41-Hb 0.50 mg mL^{-1} (red), 1.00 mg mL^{-1} (blue), 2.00 mg mL^{-1} (gray) and 5.00 mg mL^{-1} (orange). The j-E profiles show an important catalytic current that increases with the amount of MCM41-Hb. These results clearly demonstrate that Hb retains the biocatalytic properties even after sonication and integration to MWCNTs-MCM41 hybrid material. Considering that the improvements attained with 5.0 mg mL^{-1} MCM41-Hb are not significant compared to 2.00 mg mL^{-1}, we used 2.00 mg mL^{-1} MCM41-Hb for further experiments.

The comparison of Γ_{Hb} and k obtained under the optimal conditions with those reported in the literature, demonstrates that Γ_{Hb} (4.7×10^{-10} mol cm^{-2}) is higher than the one obtained at SWCNTs-Hb microbelts (Ding et al., 2010) and is almost 25 times higher than the theoretical value for a monolayer coverage (1.89×10^{-11} mol cm^{-2}), showing that a multilayer of Hb participates in the electron-transfer process in the MWCNTs-MCM41 3D-structure. The estimated k value (5.2 s^{-1}) is higher than that obtained with bioplatforms based on MWCNTs-gold nanoparticles-graphene oxide (2.61 s^{-1}) (Wang and Bi, 2014), and graphene-copper sulfide (1.58 s^{-1}) (Shi et al., 2015) hybrid materials.

3.3. Bioelectrocatalytic determination of nitrite and trichloroacetic acid

Taking advantage of the excellent enzymatic activity of hemoglobin towards different substrates and the efficient charge transfer of the heme group at the proposed bioanalytical platform, we evaluated the third-generation biosensing applications selecting two important analytes of Hb like nitrite and TCA.

High nitrite levels may have detrimental effects on the human body due to the oxidation of hemoglobin to methemoglobin, that produces cellular hypoxia (Doyle et al., 1985; Levett et al., 2011), and the formation of N-nitrosamines, which are potent carcinogens (Huang et al., 1996; Lijinsky and Epstein, 1970). As NO_2^- is widely present in the environment, beverages and food products, there is an urgent need to develop biosensors that allow the fast, sensitive and selective quantification. Considering that Hb presents nitrite reductase activity (Gladwin and Kim-Shapiro, 2008), we evaluated the usefulness of GCE/MWCNTs-MCM41-Hb for the quantification of NO_2^-. Fig. 4 depicts cyclic voltammograms obtained in N_2-saturated 0.050 M phosphate buffer solution pH 7.00 for GCE/MWCNTs-MCM41-Hb in the absence (a) and presence (b) of 1.5×10^{-2} M NO_2^-. An important enhancement of the cathodic peak current and a decrease of the anodic one are observed in the presence of nitrite, clearly demonstrating the excellent biocatalytic activity of the Hb confined to the MWCNTs-MCM41 surface. On the contrary, at GCE/MWCNTs platform this biocatalytic current is not present (inset in Fig. 4A). In order to obtain the best signal-to-noise ratio for NO_2^- amperometric detection and avoid/minimize the possible interference of easily oxidizable compounds, the selected working potential was − 0.100 V. Fig. 4B shows the amperometric response of GCE/MWCNTs-MCM41-Hb upon successive additions of $NaNO_2$ to N_2-saturated 0.050 M phosphate buffer solution pH 7.00 at − 0.100 V. The biosensor exhibits a very fast response to the changes of NO_2^- concentration, the steady-state being reached in 5 s. Under these conditions, the calibration plot for NO_2^- (Fig. 4C) shows a wide linear range between 1.0×10^{-7} M and 1.25×10^{-4} M (r^2 = 0.9997), with a sensitivity of (32.1 ± 0.1) µA mM^{-1} (or (518 ± 2) µA mM^{-1} cm^{-2}), and a detection limit of 16 nM (taken as

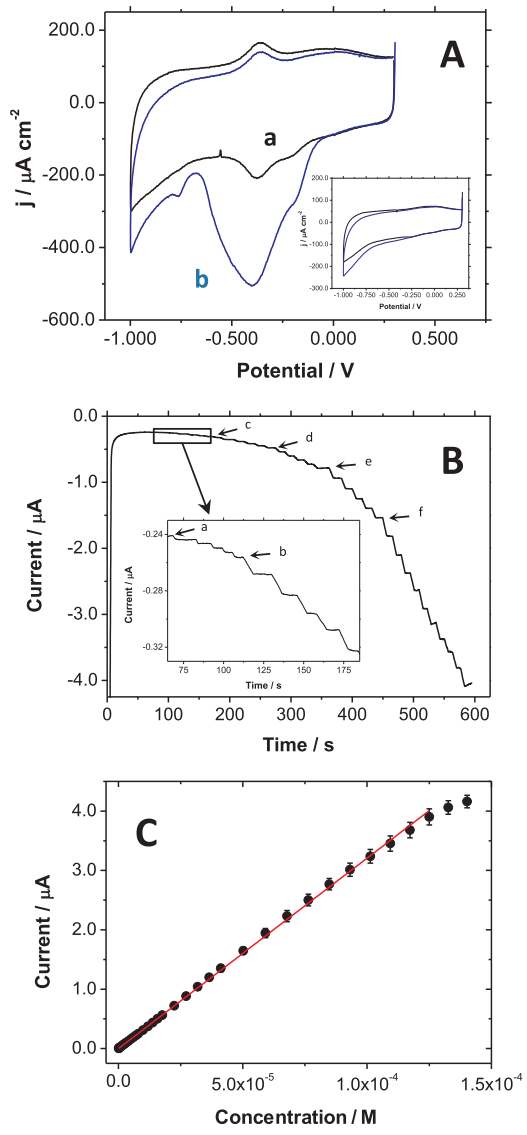

Fig. 4. Cyclic voltammograms obtained in a N_2-saturated 0.050 M phosphate buffer solution pH 7.00 in the absence (black) and presence (blue) of 1.5×10^{-2} M $NaNO_2$ at GCE/MWCNTs-MCM41-Hb (A) and GCE/MWCNTs (Inset). Scan rate: 0.100 V s^{-1}. (B) Amperometric recording for successive additions of (a) 1.0×10^{-7} M, (b) 5.0×10^{-7} M, (c) 1.0×10^{-6} M, (d) 2.0×10^{-6} M, (e) 5.0×10^{-6} M, and (f) 1.0×10^{-5} M $NaNO_2$ at GCE/MWCNTs-MCM41-Hb. Working potential: – 0.100 V. (C) Calibration plot obtained from the amperometric recording showh in Fig. 4B. (For interpretation of the references to color in this figure legend, the reader is referred to the web version of this article.)

3.3 σ/S, where σ is the standard deviation of the blank signald and S the sensitivity). This linear range is adequate to quantify the maximum contaminant level for NO_2^- in drinking water, 21.7 μM, based on the regulation of U.S. EPA (Daniel et al., 2009), and to detect anomalous serum NO_2^- levels in patients with hypertension and ischemic stroke (Gumanova et al., 2015). The sensitivities obtained from the amperometric response to NO_2^- using five different GCE/MWCNTs-MCM41-Hb biosensors prepared the same day with the same MWCNTs-MCM41-Hb dispersion gave a RSD value of 4.9%. The repeatability of GCE/MWCNTs-MCM41-Hb obtained from ten consecutive NO_2^- determinations was 7.9%. The stability of the MWCNTs-MCM41-Hb dispersion was evaluated from the NO_2^- signal using different electrodes prepared with the same dispersion stored at 4 °C. After 7 days, the signal was 95% of the original value. Table 1-SI compares the analytical performance of our biosensor with other NO_2^- biosensors reported in the last years. The linear range of our biosensor, that covers three orders of magnitude, is comparable to most of those reported in Table 1-SI. The detection limit obtained with our biosensor is lower than most of those summarized in Table 1-SI. Nitrite biosensors based on the immobilization of cytochrome c (Cyt c) at tinanium nitride nanoparticles-MWCNTs nanocomposite (MWCNTs-TiNNPs) (Haldorai et al., 2016), and on the immobilization of myoglobin (Mb) at an hybrid material of MWCNTs, poly(tyramine) and gold nanoparticles (MWCNTs-pTA-AuNPs) (Vilian et al., 2015) present detection limits lower than the one reported here. However, is important to remark that these biosensors are based on the oxidation of NO_2^- at very high potentials, and one remarkable advantage of our biosensor is the working potential, which is considerably smaller than the working potentials used in most of the reported nitrite biosensors. The total time to perform the assay from the preparation of the dispersion to the measurement was around 2 h, being the real time for the assay just few minutes.

In order to assess the broad applicability of the GCE/MWCNTs-MCM41-Hb electrochemical biointerface and taking into account the known catalytic activity of Hb towards the dechlorination of chlorinated organic compounds (COCs) (Liu et al., 2013), we also evaluated the biosensing activity of the proposed platform towards trichloroacetic acid (TCA). Even when TCA has been classified as a possible human carcinogen, solutions containing TCA as an ingredient are used for the precipitation of macromolecules and in cosmetic treatments, such as chemical peels, tattoo removal and the treatment of warts (Gao et al., 2011). Therefore, there is an increasing interest to develop biosensors for the efficient quantification of TCA. The GCE/MWCNTs-MCM41-Hb bioplatform showed good electrocatalytic ability to reduce TCA, as shown in Fig. 5A. The comparison of the potentiodynamic profile obtained in N_2-saturated 0.050 M phosphate buffer solution pH 7.00 (a) with the one obtained in the presence of 0.100 M TCA shows a significant increase in the reduction current which starts at − 0.050 V. At variance with this response, the direct reduction of TCA at GCE/MWCNTs occurs at around −0.650 V (inset in Fig. 5A), demonstrating that the presence of Hb in the hybrid material also reduces the overpotential for TCA reduction. Fig. 5B displays the amperometric response obtained at GCE/MWCNTs-MCM41-Hb biosensor at – 0.100 V for successive additions of TCA, and Fig. 5C shows the corresponding calibration curve. A fast response is observed after addition of TCA with steady-state currents reached in only 3 s. The analytical parameters are the following: linear range from 5.0×10^{-5} M to 2.7×10^{-2} M (r^2 = 0.9998), sensitivity of (197.2 ± 0.5) μA M^{-1} (or (3181 ± 8) μA M^{-1} cm^{-2}), and detection limit of 3 μM (taken as it was previously indicated). The reproducibility obtained with six different GCE/MWCNTs-MCM41-Hb biosensors prepared the same day with the same MWCNTs-MCM41-Hb dispersion was 3.7%. The repeatability for ten consecutive TCA determinations was 7.1%. The stability of the MWCNTs-MCM41-Hb dispersion was evaluated from the TCA signal obtained with biosensors prepared different days using the same dispersion stored at 4 °C. After 7 days, the signal remained in a 95%. Compared with different TCA biosensors reported in the literature (Table 1-SI), the proposed biosensor possesses the widest linear range and the detection limit is lower than most of them. As in the case of nitrite, the total time for the quantification of TCA, once prepared the dispersion/sensor was just few minutes.

The selectivity of the biosensor was evaluated in the presence of common interfering compounds such as anions, cations and small biomolecules (Fig. 3-SI). The study showed that no amperometric response was observed for the addition of 1.0×10^{-3} M $MgCl_2$, $CaCl_2$, Na_2CO_3, CH_3COOH, KCl, $NaNO_3$, $CuSO_4$ and glucose; 1.0×10^{-4} ascorbic acid (AA); 3.0×10^{-4} M uric acid (UA); and 3.0×10^{-6} M dopamine (Dop), indicating that the proposed biosensor presents very good selectivity.

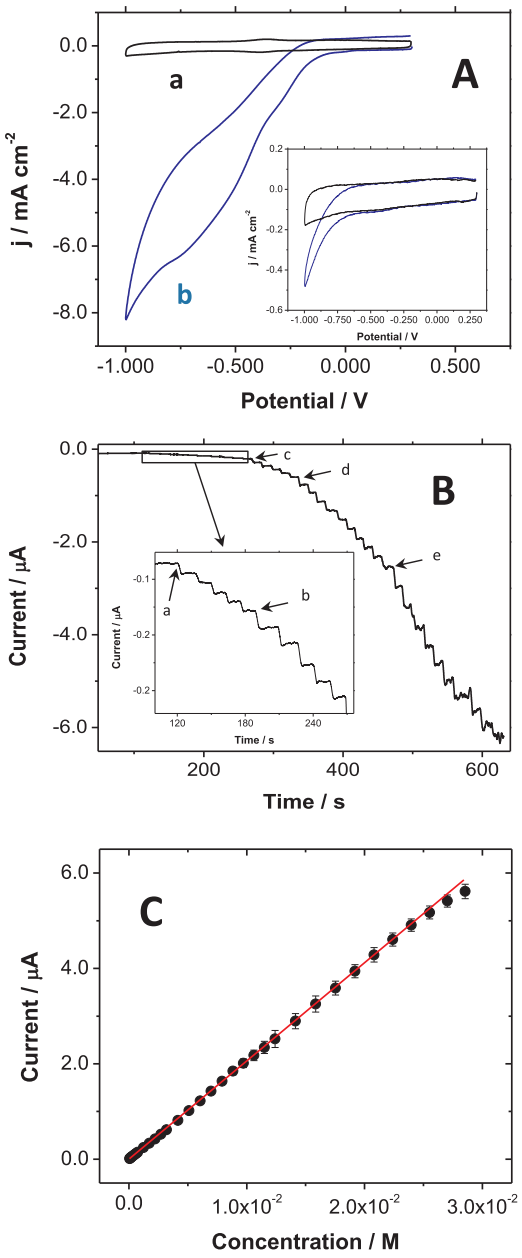

Fig. 5. Cyclic voltammograms obtained in a N_2-saturated 0.050 M phosphate buffer solution pH 7.00 in the absence (black) and presence (blue) of 0.100 M TCA at GCE/MWCNTs-MCM41-Hb (A) and GCE/MWCNTs (Inset). Scan rate: 0.100 V s^{-1}. (B) Amperometric recording for successive additions of (a) 5.0×10^{-5} M, (b) 1.0×10^{-4} M, (c) 5.0×10^{-4} M, (d) 1.0×10^{-3} M and 2.0×10^{-3} M TCA at GCE/MWCNTs-MCM41-Hb. Working potential: –0.100 V. (C) Calibration plot obtained from the amperometric recording shown in Fig. 5B. (For interpretation of the references to color in this figure legend, the reader is referred to the web version of this article.)

3.4. Real sample analysis

GCE/MWCNTs-MCM41-Hb biosensor was used for the determination of NO_2^- and TCA in spiked tap water samples. The mean recoveries ranged between 99% and 100% being the relative standard deviations lower than 10% (Table 1). These results confirmed the usefullness of the developed GCE/MWCNTs-MCM41-Hb biosensor for the determination of NO_2^- and TCA in tap water samples.

Table 1
Analytical application of GCE/MWCNTs-MCM41-Hb for the quantification of NO_2^- in tap water spiked with 20 µM and 200 µM $NaNO_2$, and for the quantification of TCA in tap water spiked with 10 µM TCA.

Sample	*$NaNO_2$ (µM)*		*RSD (%)*	*Recovery (%)*
	Spiked	*Found*		
Tap water	0	–	–	–
	20	20 ± 1	5.0	100 ± 5
	200	200 ± 4	2.0	100 ± 2
Sample	*TCA (mM)*		*RSD (%)*	*Recovery (%)*
	Spiked	*Found*		
Tap water	0	–	–	–
	10	9.9 ± 0.9	9.1	99 ± 9

4. Conclusions

In summary, we proposed a new third-generation biosensor based on the use of a nanohybrid prepared through the successful association of Nafion-MWCNT with mesoporous silica MCM41 functionalized with Hb. The loading capacity of the silica particles, the catalytic activity of MWCNTs and the intimate contact of the protein with MWCNTs allowed the efficient electron transfer of Hb and the successful application of the resulting nanobioanalytical platform for nitrite and trichloroacetic acid biosensing. The new biosensor represents an interesting analytical tool for the development of easy-to-prepare, fast, and sensitive biosensors for environmental application.

Acknowledgements

Financial support from CONICET, ANPCyT, SECyT-UNC (Argentina) and Spanish Ministry of Economy and Competitiveness (projects CTQ2014-58989-P and CTQ2015-71936-REDT) is acknowledged.

Appendix A. Supplementary material

Supplementary data associated with this article can be found in the online version at http://dx.doi.org/10.1016/j.bios.2018.04.004.

References

Abraham, S., Srivastava, S., Kumar, V., Pandey, S., Rastogi, K., Nirala, N.R., Kashyap, S., Srivastava, S.K., Singh, V.N., Ganesan, V., Saxena, P.S., Srivastava, A., 2015. Enhanced electrochemical biosensing efficiency of silica particles supported on partially reduced graphene oxide for sensitive detection of cholesterol. J. Electroanal. Chem. 757, 65–72. http://dx.doi.org/10.1016/j.jelechem.2015.09.016.

Baccarin, M., Janegitz, B.C., Berté, R., Campanhã, F., Banks, C.E., Fatibello-Filho, O., Zucolotto, V., 2015. Direct electrochemistry of hemoglobin and biosensing for hydrogen peroxide using a film containing silver nanoparticles and poly (amidoamine) dendrimer. Mater. Sci. Eng. C 58, 97–102. http://dx.doi.org/10.1016/j.msec.2015.08.013.

Bagheri, H., Ranjbari, E., Amiri-Aref, M., Hajian, A., Ardakani, Y.H., Amidi, S., 2016. Modified fractal iron oxide magnetic nanostructure: a novel and high performance platform for redox protein immobilization, direct electrochemistry and bioelectrocatalysis application. Biosens. Bioelectron. 85, 814–821. http://dx.doi.org/10.1016/j.bios.2016.05.097.

Boujakhrout, A., Sánchez, E., Díez, P., Sánchez, A., Martínez-Ruiz, P., Parrado, C., Pingarrón, J.M., Villalonga, R., 2015. Single-walled carbon nanotubes/Au – mesoporous silica janus nanoparticles as building blocks for the preparation of a bienzyme biosensor. ChemElectroChem 2, 1735–1741. http://dx.doi.org/10.1002/celc.201500244.

Chen, G., Sun, H., Hou, S., 2016. Electrochemistry and electrocatalysis of myoglobin immobilized in sulfonated graphene oxide and nafion films. Abalytical Biochem. 502, 43–49. http://dx.doi.org/10.1016/j.ab.2016.03.003.

Chen, X., Zhang, Q., Qian, C., Hao, N., Xu, L., Yao, C., 2014. Electrochemical aptasensor for mucin 1 based on dual signal amplification of poly(o-phenylenediamine) carrier and functionalized carbon nanotubes tracing tag. Biosens. Bioelectron. 64, 485–492. http://dx.doi.org/10.1016/j.bios.2014.09.052.

Dai, Z., Liu, S., Ju, H., Chen, H., 2004. Direct electron transfer and enzymatic activity of hemoglobin in a hexagonal mesoporous silica matrix. Biosens. Bioelectron. 19,

861–867. http://dx.doi.org/10.1016/j.bios.2003.08.024|.
Daniel, W.L., Han, M.S., Lee, J.S., Mirkin, C. a., 2009. Colorimetric nitrite and nitrate detection with gold nanoparticle probes and kinetic end points. J. Am. Chem. Soc. 131, 6362–6363. http://dx.doi.org/10.1021/ja901609k.
Das, P., Das, M., Chinnadayyala, S.R., Singha, I.M., Goswami, P., 2016. Recent advances on developing 3rd generation enzyme electrode for biosensor applications. Biosens. Bioelectron. 79, 386–397. http://dx.doi.org/10.1016/j.bios.2015.12.055.
Devineau, S., Zargarian, L., Renault, J.P., Pin, S., 2017. Structure and function of adsorbed hemoglobin on silica nanoparticles: relationship between the adsorption process and the oxygen binding properties. Langmuir 33, 3241–3252. http://dx.doi.org/10.1021/acs.langmuir.6b04281.
Ding, L., You, J., Kong, R., Qu, F., 2013. Signal amplification strategy for sensitive immunoassay of prostate specific antigen (PSA) based on ferrocene incorporated polystyrene spheres. Anal. Chim. Acta 793, 19–25. http://dx.doi.org/10.1016/j.aca.2013.07.054.
Ding, Y., Wang, Y., Lei, Y., 2010. Direct electrochemistry and electrocatalysis of novel single-walled carbon nanotubes-hemoglobin composite microbelts-towards the development of sensitive and mediator-free biosensor. Biosens. Bioelectron. 26, 390–397. http://dx.doi.org/10.1016/j.bios.2010.07.124.
Doyle, M.P., Herman, J.G., Dykstra, R.L., 1985. Autocatalytic oxidation of hemoglobin induced by nitrite: activation and chemical inhibition. J. Free Radic. Biol. Med. 1, 145–153. http://dx.doi.org/10.1016/0748-5514(85)90019-4.
Eguílaz, M., Gutiérrez, A., Rivas, G., 2016. Non-covalent functionalization of multi-walled carbon nanotubes with cytochrome c: enhanced direct electron transfer and analytical applications. Sens. Actuators B Chem. B Chem. 225, 74–80. http://dx.doi.org/10.1016/j.snb.2015.11.011.
Eguílaz, M., Villalonga, R., Pingarrón, J.M., Ferreyra, N.F., Rivas, G.A., 2015. Functionalization of bamboo-like carbon nanotubes with 3-mercaptophenylboronic acid-modified gold nanoparticles for the development of a hybrid glucose enzyme electrochemical biosensor. Sens. Actuators, B Chem. 216, 629–637. http://dx.doi.org/10.1016/j.snb.2015.03.112.
Eguílaz, M., Villalonga, R., Yáñez-Sedeño, P., Pingarrón, J.M., 2011. Designing electrochemical interfaces with functionalized magnetic. Anal. Chem. 83, 7807–7814.
Everson, T.S., Souto, D.E., Barragan, J.F.G., Moraes, A.C., Kubota, L.T., 2017. Electrochemical biosensors in point-of-care devices: recent advances and future trends. ChemElectroChem 4, 778–794. http://dx.doi.org/10.1002/celc.201600758.
Feng, X., Li, R., Hu, C., Hou, W., 2011. Direct electron transfer and electrocatalysis of hemoglobin immobilized on graphene – Pt nanocomposite. J. Electroanal. Chem. 657, 28–33. http://dx.doi.org/10.1016/j.jelechem.2011.03.004.
Gao, Y.-C., Xi, K., Wang, W.-N., Jia, X.-D., Zhu, J.-J., 2011. A novel biosensor based on a gold nanoflowers/hemoglobin/carbon nanotubes modified electrode. Anal. Methods 3, 2387–2391. http://dx.doi.org/10.1039/c1ay05378g.
Ghodsi, J., Hajian, A., Rafati, A.A., Shoja, Y., Yurchenko, O., Urban, G., 2016. Electrostatically immobilized hemoglobin on silica-coated magnetic nanoparticles for simultaneous determination of dopamine, uric acid, and folic acid. J. Electrochem. Soc. 163, B609–B616. http://dx.doi.org/10.1149/2.0481613jes.
Gladwin, M.T., Kim-Shapiro, D.B., 2008. The functional nitrite reductase activity of the heme-globins. Blood 112, 2636–2647. http://dx.doi.org/10.1182/blood-2008-01-115261.2636.
Gumanova, N.G., Teplova, N.V., Ryabchenko, A.U., Denisov, E.N., 2015. Serum nitrate and nitrite levels in patients with hypertension and ischemic stroke depend on diet: a multicenter study. Clin. Biochem. 48, 29–32. http://dx.doi.org/10.1016/j.clinbiochem.2014.10.010.
Haldorai, Y., Hwang, S.K., Gopalan, A.I., Huh, Y.S., Han, Y.K., Voit, W., Sai-Anand, G., Lee, K.P., 2016. Direct electrochemistry of cytochrome c immobilized on titanium nitride/multi-walled carbon nanotube composite for amperometric nitrite biosensor. Biosens. Bioelectron. 79, 543–552. http://dx.doi.org/10.1016/j.bios.2015.12.054.
Hasanzadeh, M., Shadjou, N., Guardia, M. de la, Eskandani, M., Sheikhzadeh, P., 2012. Mesoporous silica-based materials for use in biosensors. TrAC - Trends Anal. Chem. 33, 117–129. http://dx.doi.org/10.1016/j.trac.2011.10.011.
Hasanzadeh, M., Shadjou, N., Omidinia, E., Eskandani, M., de la Guardia, M., 2013. Mesoporous silica materials for use in electrochemical immunosensing. TrAC - Trends Anal. Chem. http://dx.doi.org/10.1016/j.trac.2012.12.017.
Huang, Y.G., Ji, J.D., Hou, Q.N., 1996. A study on carcinogenesis of endogenous nitrite and nitrosamine, and prevention of cancer. Mutat. Res. 358, 7–14. http://dx.doi.org/10.1016/0027-5107(96)00087-5.
Iminova, Y.V., Tananaiko, O.Y., Rozhanchuk, T.S., Gruzina, T.G., Reznichenko, L.S., Malysheva, M.L., Ulberg, Z.R., 2015. Electrodes modified by a biocomposite film based on silica and gold nanoparticles for the determination of glucose. Journal of Analytical Chemistry 70, 1247–1253. http://dx.doi.org/10.1134/S1061934815080109.
Khan, A.Y., Noronha, S.B., Bandyopadhyaya, R., 2016. Superior performance of a carbon-paste electrode based glucose biosensor containing glucose oxidase enzyme in mesoporous silica powder. Adv. Powder Technol. 27, 85–92. http://dx.doi.org/10.1016/j.apt.2015.11.003.
Laviron, E., 1979a. The use of linear potential sweep voltammetry and of A.C. voltammetry for the study of the surface electrochemical reaction of strongly adsorbed systems and of redox modified electrodes. J. Electroanal. Chem. 100, 263–270.
Laviron, E., 1979b. General expression of the linear potential sweep voltammogram in the case of diffusionless electrochemical systems. J. Electroanal. Chem. 101, 19–28.
Levett, D.Z., Fernandez, B.O., Riley, H.L., Martin, D.S., Mitchell, K., Leckstrom, C.A., Ince, C., Whipp, B.J., Mythen, M.G., Montgomery, H.E., Grocott, M.P., Feelisch, M., 2011. The role of nitrogen oxides in human adaptation to hypoxia. Sci. Rep. 1, 109. http://dx.doi.org/10.1038/srep00109.
Li, J., Xiong, Z., Zhou, L., Han, X., Liu, H., 2010. Effects of pore structure of mesoporous silicas on the electrochemical properties of hemoglobin. Microporous Mesoporous Mater. 130, 333–337. http://dx.doi.org/10.1016/j.micromeso.2009.11.031.
Lijinsky, W., Epstein, S.S., 1970. Nitrosamines as environmental carcinogens. Nature 225, 21–23.
Liu, Q., Yu, J., Xu, Y., Wang, J., Ying, L., Song, X., Zhou, G., Chen, J., 2013. Bioelectrocatalytic dechlorination of trichloroacetic acid at gel-immobilized hemoglobin on multiwalled carbon nanotubes modified graphite electrode: kinetic modeling and reaction pathways. Electrochim. Acta 92, 153–160. http://dx.doi.org/10.1016/j.electacta.2013.01.015.
Moerz, S.T., Huber, P., 2015. PH-dependent selective protein adsorption into mesoporous silica. J. Phys. Chem. C 119, 27072–27079. http://dx.doi.org/10.1021/acs.jpcc.5b09606.
Pabbi, M., Mittal, S.K., 2017. Electrochemical algal biosensor based on silica coated ZnO quantum dots for selective determination of acephate. Anal. Methods 9, 1672–1680. http://dx.doi.org/10.1039/C7AY00111H.
Qu, F., Yang, M., Rasooly, A., 2016. Dual signal amplification electrochemical biosensor for monitoring the activity and inhibition of the Alzheimer's related protease β-secretase. Anal. Chem. 88, 10559–10565. http://dx.doi.org/10.1021/acs.analchem.6b02659.
Shi, F., Zheng, W., Wang, W., Hou, F., Lei, B., Sun, Z., Sun, W., 2015. Application of graphene-copper sulfide nanocomposite modified electrode for electrochemistry and electrocatalysis of hemoglobin. Biosens. Bioelectron. 64, 131–137. http://dx.doi.org/10.1016/j.bios.2014.08.064.
Suteewong, T., Sai, H., Cohen, R., Wang, S., Bradbury, M., Baird, B., Gruner, S.M., Wiesner, U., 2011. Highly aminated mesoporous silica nanoparticles with cubic pore structure. J. Am. Chem. Soc. 133, 172–175. http://dx.doi.org/10.1021/ja1061664.
Taurino, I., Sanzó, G., Antiochia, R., Tortolini, C., Mazzei, F., Favero, G., De Micheli, G., Carrara, S., 2016. Recent advances in third generation biosensors based on Au and Pt nanostructured electrodes. TrAC - Trends Anal. Chem. 79, 151–159. http://dx.doi.org/10.1016/j.trac.2016.01.020.
Urabe, Y., Shiomi, T., Itoh, T., Kawai, A., Tsunoda, T., Mizukami, F., Sakaguchi, K., 2007. Encapsulation of hemoglobin in mesoporous silica (FSM) - enhanced thermal stability and resistance to denaturants. ChemBioChem 8, 668–674. http://dx.doi.org/10.1002/cbic.200600486.
Vilian, A.T.E., Veeramani, V., Chen, S.-M., Madhu, R., Kwak, C.H., Huh, Y.S., Han, Y.-K., 2015. Immobilization of myoglobin on Au nanoparticle-decorated carbon nanotube/polytyramine composite as a mediator-free H2O2 and nitrite biosensor. Sci. Rep. http://dx.doi.org/10.1038/srep18390.
Walcarius, A., Mandler, D., Cox, J.A., Collison, M., Lev, O., 2005. Exciting new directions in the intersection of functionalized sol – gel materials with electrochemistry. J. Mater. Chem. 15, 3663–3689. http://dx.doi.org/10.1039/b504839g.
Walcarius, A., Minteer, S.D., Wang, J., Lin, Y., Merkoçi, A., 2013. Nanomaterials for bio-functionalized electrodes: recent trends. J. Mater. Chem. B 1, 4878–4908. http://dx.doi.org/10.1039/c3tb20881h.
Wang, Y., Bi, C.Y., 2014. A novel nitrite biosensor based on direct electron transfer of hemoglobin immobilized on a graphene oxide/Au nanoparticles/multiwalled carbon nanotubes nanocomposite film. RSC Adv. 4, 31573–31580. http://dx.doi.org/10.1039/C4ra05237d.
Wang, Y., Huang, K., Wu, X., 2017a. Recent advances in transition-metal dichalcogenides based electrochemical biosensors: a review. Biosens. Bioelectron. 97, 305–316. http://dx.doi.org/10.1016/j.bios.2017.06.011.
Wang, L., Li, J., Feng, M., Min, L., Yang, J., Yu, S., Zhang, Y., Hu, X., Yang, Z., 2017b. Perovskite-type calcium titanate nanoparticles as novel matrix for designing sensitive electrochemical biosensing. Biosens. Bioelectron. 96, 220–226. http://dx.doi.org/10.1016/j.bios.2017.05.004.
Wu, S.-H., Mou, C.-Y., Lin, H.-P., 2013. Synthesis of mesoporous silica nanoparticles. Chem. Soc. Rev. 42, 3862. http://dx.doi.org/10.1039/c3cs35405a.
Yang, C., Denno, M.E., Pyakurel, P., Venton, B.J., 2015a. Recent trends in carbon nanomaterial-based electrochemical sensors for biomolecules: a review. Anal. Chim. Acta 887, 17–37. http://dx.doi.org/10.1016/j.aca.2015.05.049.
Yang, N., Chen, X., Ren, T., Zhang, P., Yang, D., 2015b. Carbon nanotube based biosensors. Sens. Actuators B Chem. Part 690–715. http://dx.doi.org/10.1016/j.snb.2014.10.040.
Ye, H., Guo, Z., Peng, M., Cai, C., Chen, Y., Cao, Y., Zhang, W., 2016. Methyl parathion degrading enzyme-based nano-hybrid biosensor for enhanced methyl parathion recognition. Electroanalysis 28, 1591–1596. http://dx.doi.org/10.1002/elan.201501102.
Zhang, J., Chai, Y., Yuan, R., Yuan, Y., Bai, L., Xie, S., 2013. A highly sensitive electrochemical aptasensor for thrombin detection using functionalized mesoporous silica@multiwalled carbon nanotubes as signal tags and. Analyst 138, 6938–6945. http://dx.doi.org/10.1039/c3an01587d.
Zhao, Y., Zheng, Y., Kong, R., Xia, L., Qu, F., 2016. Ultrasensitive electrochemical immunosensor based on horseradish peroxidase (HRP)-loaded silica-poly(acrylic acid) brushes for protein biomarker detection. Biosens. Bioelectron. 75, 383–388. http://dx.doi.org/10.1016/j.bios.2015.08.065.
Zhu, C., Yang, G., Li, H., Du, D., Lin, Y., 2015. Electrochemical sensors and biosensors based on nanomaterials and nanostructures. Anal. Chem. 87, 230–249.